Atmos. Chem. Phys. Discuss., 14, 21749–21784, 2014
www.atmos-chem-phys-discuss.net/14/21749/2014/
doi:10.5194/acpd-14-21749-2014

Atmospheric Chemistry and Physics Discussions

Evaluation of a regional air quality model using satellite column NO_2: treatment of observation errors and model boundary conditions and emissions

R. J. Pope[1], M. P. Chipperfield[1], N. H. Savage[2], C. Ordóñez[2], L. S. Neal[2], L. A. Lee[1], S. S. Dhomse[1], and N. A. D. Richards[1]

[1]School of Earth and Environment, University of Leeds LS2 9JT, Leeds, UK
[2]Met Office, Exeter, UK

Received: 1 July 2014 – Accepted: 13 July 2014 – Published: 26 August 2014

Correspondence to: R. Pope (eerjp@leeds.ac.uk)

Published by Copernicus Publications on behalf of the European Geosciences Union.

Abstract

We compare tropospheric column NO_2 between the UK Met Office operational Air Quality in the Unified Model (AQUM) and satellite observations from the Ozone Monitoring Instrument (OMI) for 2006. Column NO_2 retrievals from satellite instruments are prone to large uncertainty from random, systematic and smoothing errors. We present an algorithm to reduce the random error of time-averaged observations, once smoothing errors have been removed with application of satellite averaging kernels to the model data. This reduces the total error in seasonal mean columns by 30–90 %, which allows critical evaluation of the model. The standard AQUM configuration evaluated here uses chemical lateral boundary conditions (LBCs) from the GEMS (Global and regional Earth-system Monitoring using Satellite and in-situ data) reanalysis. In summer the standard AQUM overestimates column NO_2 in northern England and Scotland, but underestimates it over continental Europe. In winter, the model overestimates column NO_2 across the domain. We show that missing heterogeneous hydrolysis of N_2O_5 in AQUM is a significant sink of column NO_2 and that the introduction of this process corrects some of the winter biases. The sensitivity of AQUM summer column NO_2 to different chemical LBCs and NO_x emissions datasets are investigated. Using Monitoring Atmospheric Composition and Climate (MACC) LBCs increases AQUM O_3 concentrations compared with the default GEMS LBCs. This enhances the NO_x-O_3 coupling leading to increased AQUM column NO_2 in both summer and winter degrading the comparisons with OMI. Sensitivity experiments suggest that the cause of the remaining northern England and Scotland summer column NO_2 overestimation is the representation of point source (power station) emissions in the model.

1 Introduction

Air quality has a major influence on the UK both socially and economically. It can result in approximately 50 000 premature deaths per year and an average reduction in life

ACPD
14, 21749–21784, 2014

expectancy of 7–8 months (HoC, 2010). Air pollution health effects include lung disease and cancer, cardiovascular problems, asthma and eye irritation (WHO, 2011). In 2005 poor UK air quality cost £ (€) 8.5 (10.7)–20.2 (25.5) billion and between 2007–2008 there were 74 000 asthma-related hospital admissions. Overall, these air quality-asthma incidents cost society £ (€) 2.3 (2.9) billion (HoC, 2010). Poor air quality associated with ozone concentrations over 40 ppbv can also significantly reduce crop yields e.g. Hollaway et al. (2012).

Therefore, regional models have been developed to predict hazardous levels of air pollution to help inform the public and to allow local authorities to take action to reduce/accommodate the respective health risks/effects. Air quality models have mainly been evaluated against surface observations, e.g. Savage et al. (2013). However, recently such models have also been compared with satellite observations, taking advantage of the better spatial coverage despite the potentially large error of individual observations. In the past NO_2 satellite data has been compared mainly with global atmospheric chemistry models (e.g. Velders et al., 2001; Lauer et al., 2002; Van Noije et al., 2006). However, more recently, other studies have used satellite data to evaluate models on a regional scale. Savage et al. (2008) investigated European tropospheric column NO_2 interannual variability (IAV), 1996–2000, by comparing GOME with the TOMCAT chemical transport model (CTM) (Monks et al., 2012). The best comparisons were found in the JFM and AMJ seasons, especially over western Europe. They also found that synoptic meteorology had more influence on NO_2 IAV than NO_x emissions did.

Huijnen et al. (2010) compared Ozone Monitoring Instrument (OMI) tropospheric column NO_2 against a European global-regional air quality model ensemble median for 2008–2009. The ensemble compared better with the OMI data than any one model, with good agreement over the urban hotspots. Overall, the spread in the models was greatest in the summer (with deviations from the mean OMI tropospheric column in the range 40–62 %), due to the more active NO_x chemistry in this season and the differences in chemistry schemes among the contributing models, when compared to

ACPD
14, 21749–21784, 2014

winter (20–34 %). Several of the regional models successfully detected the shipping lanes seen by OMI.

Han et al. (2011) investigated tropospheric column NO_2 over the Korean Peninsula through comparisons between OMI data and the Community Multi-scale Air Quality Model (CMAQ) (Foley et al., 2010). In summer North and South Korea had similar column NO_2 from both model and observations. However, in winter South Korea, a more developed nation with greater infrastructure, had significantly greater NO_2 concentrations than North Korea. Overall, CMAQ overestimated OMI NO_2 concentrations by factors of 1.38–1.87 and 1.55–7.46 over South and North Korea, respectively.

Other studies investigating regional tropospheric column NO_2 through model simulations and satellite observations include Blond et al. (2007), Boersma et al. (2009) and Curier et al. (2014). Blond et al. (2007) compared CHIMERE 3-D CTM and SCIAMACHY column NO_2 over western Europe with good agreement with winter and summer correlations of 0.79 and 0.82, respectively. Boersma et al. (2009) used the GEOS-Chem 3-D CTM to explain the seasonal cycle in SCIAMACHY and OMI column NO_2 over Israeli cities, with larger photochemical loss of NO_2 in summer than winter. And Curier et al. (2014) used a synergistic of OMI and the LOTOS-EUROS 3-D CTM to evaluate NO_x trends finding negative trends of 5–6 % over western Europe.

The UK Met Office's Air Quality in the Unified Model (AQUM) is used for short operational chemical weather forecasts of UK air quality. Savage et al. (2013) performed the first evaluation of the AQUM operational forecast for the period May 2010–April 2011 by using surface O_3, NO_2 and particulate matter observations from the UK Automated Urban and Rural Network (AURN) (DEFRA, 2012). Among other model-observation metrics they used the mean bias (MB), root mean square error (RMSE), modified normalised mean bias (MNMB) and the Fractional Gross Error (FGE) (Seigneur et al., 2000). See the Appendix for the definition of these metrics.

Savage et al. (2013) found that AQUM overestimated O_3 by 8.38 $\mu g\,m^{-3}$ (MNMB = 0.12), with a positive bias at urban sites but no systematic bias at rural sites. The model-observation correlation was reasonably high at 0.68. For NO_2, there was

ACPD
14, 21749–21784, 2014

a bias of $-6.10\,\mu g\,m^{-3}$, correlation of 0.57 and MNMB of −0.26. At urban sites there was a large negative bias while rural sites had marginal positive biases. The coarse resolution of AQUM (12 km) led to an underestimation at urban sites because the model NO_x emissions are instantaneously spread over the entire grid box. The particulate matter (PM_{10}) prediction skill was lower with a correlation and bias of 0.52 and $-9.17\,\mu g\,m^{-3}$, respectively.

The aim of this paper is to evaluate AQUM using satellite atmospheric trace gas observations. The Met Office has previously compared the skill of AQUM only against AURN surface measurements, which in the case of NO_2 are not specific and include contributions from other oxidised nitrogen compounds (see Savage et al. (2013), and references therein). Therefore, for better spatial model-observation comparisons and to minimise the effect of measurement interferences, we use satellite observations over the UK. We focus on tropospheric column NO_2 data from OMI for the summer (April–September) and winter (January–March, October–December) periods of 2006. Section 2 describes the OMI satellite data used and gives a detailed account of our error analysis which determines how we can use satellite data to test AQUM. Section 3 describes AQUM and the model experiments performed. Results from the model-observations comparisons are given in Sect. 4. Section 5 presents our conclusions.

2 Satellite data

OMI is aboard NASA's EOS-Aura satellite and has an approximate London daytime overpass at 13:00 LT. It is a nadir-viewing instrument with a pixel size of 312 km^2 and 3240 km^2 along track and across track, respectively (Boersma et al., 2008). We have taken the DOMINO tropospheric column NO_2 product, version 2.0, from the TEMIS (Tropospheric Emissions Monitoring Internet Service) website, http://www.temis.nl/airpollution/no2.html (Boersma et al., 2011b, a). We have binned NO_2 swath data from 1 January to 31 December 2006 onto a daily 13:00 LT 0.25° × 0.25° grid between 43–63° N and 20° W–20° E. All satellite retrievals have been quality controlled, and re-

ACPD
14, 21749–21784, 2014

trievals/pixels with geometric cloud cover greater than 20 % and poor quality data flags (flag = −1) were removed. The product uses the algorithm of Braak (2010) to identify OMI pixels affected by row anomalies and sets the data flags to −1. We also filter these out in this study. Even though OMI has an approximate 13:00 LT London overpass, we used all OMI retrievals in the domain between 11:00 and 15:00 LT to get more extensive spatial coverage. Several studies have validated OMI column NO_2 against surface and aircraft measurements of tropospheric column NO_2. Irie et al. (2008) compared OMI and with ground based MAX-DOAS retrievals in the Mount Tai Experiment (2006). They found the standard OMI product (version 3) overestimated the MAX-DOAS measurements by approximately 1.6×10^{15} molecules cm^{-2} (20 %), but within the OMI uncertainty limits. Boersma et al. (2008) compared the near real time (NRT) OMI product (version 0.8) with aircraft measurements in the INTEX-B campaign. Overall, they found a good correlation (0.69) between OMI and the aircraft column NO_2, with no significant biases. Therefore, we have confidence in the OMI column NO_2 and use it for evaluation of our model.

2.1 Satellite averaging kernels

Eskes and Boersma (2003) define the averaging kernel (AK) to be a relationship between the retrieved quantities and the true distribution of the tracer. In other words, the satellite instrument's capability to retrieve a quantity is a function of altitude. For instance, the instrument may be more or less sensitive retrieving a chemical species near the boundary layer than in the stratosphere. Therefore, since satellite retrievals and model vertical profiles are not directly comparable, the AK (or weighting function) is applied to the model data, so the sensitivity of the satellite is accounted for in the comparisons. The AK comes in different forms for different retrieval methods. For the Differential Optical Absorption Spectroscopy (DOAS) method, the AK is in the form of a column vector, while in Optimal Estimation, the AK is a matrix, whose dimensions depend on the number of pressure levels in the retrieval process.

ACPD
14, 21749–21784, 2014

The OMI retrievals use the DOAS technique and the AK is a column vector. Following Huijnen et al. (2010) and the OMI documentation (Boersma et al., 2011a), the AKs are applied to the model as:

$$y = A \cdot x \tag{1}$$

where y is the total column, A is the AK and x is the vertical model profile. However, here the tropospheric column is needed:

$$y_{\text{trop}} = A_{\text{trop}} \cdot x_{\text{trop}} \tag{2}$$

where A_{trop} is:

$$A_{\text{trop}} = A \cdot \frac{\text{AMF}}{\text{AMF}_{\text{trop}}} \tag{3}$$

AMF is the atmospheric air mass factor and AMF_{trop} is the tropospheric air mass factor. For the OMI product, Huijnen et al. (2010) state the AK tends to be lower than 1 in the lower troposphere (e.g. 0.2–0.7 up to 800 hPa) and greater than 1 in the mid-upper troposphere. Therefore, the OMI AKs reduce model NO_2 subcolumns in the lower troposphere and increase them in the mid-upper troposphere (Huijnen et al., 2010). Figure 1 shows example tropospheric AKs for summer and winter profiles over London (urban – higher column NO_2) and Dartmoor (rural area in southwest England – lower column NO_2), which have been coloured by their respective tropospheric AMF. In the lower troposphere for both seasons and locations the tropospheric AKs range around 0–1. However, in the mid-upper troposphere, the London tropospheric AKs tend to be greater than Dartmoor in both seasons. London tropospheric AKs are most pronounced in winter, with many tropospheric AKs over 8, while in the summer they range around 1–8. In both seasons, the tropospheric AMF is biggest, 5–6, in the lower range tropospheric AKs, 0–1, and smaller, 0–1.5 as the tropospheric AKs range increases, over 2. If the tropospheric AMFs are small (i.e. near 0 suggesting the majority of the

ACPD
14, 21749–21784, 2014

NO_2 is within the lower layers of the London boundary layer; also small tropospheric AKs there), from Eq. (3), as the full atmospheric AKs naturally increase with altitude, the tropospheric AMFs will return larger tropospheric AKs. Also, in winter over London, the shallower boundary layer with trap larger winter emissions of NO_2 closer to the surface. Therefore, the tropospheric AMF will be smaller and the winter mid-upper tropospheric AKs will be larger as seen in Fig. 1. Over Dartmoor, the AKs show less seasonal variation and the majority range around 1–6 for both summer and winter. This is also seen in the tropospheric AMF, which ranges between approximately 0–6, but has no clear pattern in the Dartmoor tropospheric AKs, in both seasons.

2.2 Differential optical absorption spectroscopy NO_2 retrieval error

The DOAS retrievals are subject to random, systematic and smoothing errors in the retrieval process. Random (quasi-systematic) errors include fitting errors, cloud errors, instrument noise and signal corruption. Systematic errors include absorption cross-sections, surface albedo and stratospheric correction uncertainties. Finally, smoothing errors include biases in the a priori profiles and sensitivity of the satellite when recording the slant column through the atmosphere. If multiple retrievals are averaged together, as in this study, the random errors will partially cancel leading to the random error being reduced by a factor of $\frac{1}{\sqrt{N}}$ (where N is the number of retrievals).

In contrast, systematic errors are unaffected by cancelling through averaging. In the following section we investigate the different error components of the satellite retrievals and derive an expression for the error in the averaged retrievals. This methodology should give smaller errors which are more representative of the time-averaged retrieval error and so allow a stricter test of the model. Boersma et al. (2004) describe the error in the DOAS NO_2 retrievals as:

$$\sigma^2_{\text{trop}} = \left(\frac{\sigma_{\text{total}}}{\text{AMF}_{\text{trop}}}\right)^2 + \left(\frac{\sigma_{\text{strat}}}{\text{AMF}_{\text{trop}}}\right)^2 + \left(\frac{(X_{\text{total}} - X_{\text{strat}})\,\sigma_{\text{AMF}_{\text{trop}}}}{\text{AMF}^2_{\text{trop}}}\right)^2 \quad (4)$$

ACPD
14, 21749–21784, 2014

where σ_{trop}, σ_{strat} and σ_{total} are the uncertainties in the tropospheric, stratospheric and total slant columns, respectively. AMF_{trop} is the tropospheric air mass factor, $\sigma_{AMF_{trop}}$ is the error in the tropospheric air mass factor, X_{total} is the total slant column and X_{strat} is the stratospheric slant column.

σ_{total} is made up of both random and systematic error, where the random error component can be reduced by $\frac{1}{\sqrt{N}}$. We assume that the systematic and random errors can be combined in quadrature. In Eq. (6) there are two terms for σ_{total}; $\sigma_{total_{ran}}$ and $\sigma_{total_{sys}}$, which are the random and systematic error components of the total slant column, respectively. Boersma et al. (2004) state that $\sigma_{total_{sys}}$ can be expressed as $\sigma_{total_{sys}} = 0.03 X_{total}$. We treat σ_{strat} here as systematic as both the OMI standard and DOMINO products estimate the stratospheric slant column using TM4 chemistry-transport model simulations and data assimilation (Dirksen et al., 2011). According to the DOMINO OMI product documentation (which references Boersma et al., 2004, 2007; Dirksen et al., 2011), the error in the stratospheric slant column is estimated to be 0.25×10^{15} molecules cm^{-2} in all cases.

Boersma et al. (2004) state that the tropospheric column is calculated as:

$$N_{trop} = \frac{X_{total} - X_{strat}}{AMF_{trop}} \quad (5)$$

where N_{trop} is the vertical tropospheric column and can be substituted, including the σ_{total} and σ_{strat} estimates, into Eq. (4). This leads to:

$$\sigma_{trop}^2 = \left(\frac{\sigma_{total_{ran}}}{AMF_{trop}}\right)^2 + \left(\frac{0.03 X_{total}}{AMF_{trop}}\right)^2 + \left(\frac{0.25 \times 10^{15}}{AMF_{trop}}\right)^2 + \left(\frac{N_{trop}\sigma_{AMF_{trop}}}{AMF_{trop}}\right)^2 \quad (6)$$

σ_{trop} is reduced in the model-satellite comparisons when the AK is applied to the model data. Therefore, the error product, $\sigma_{trop_{ak}}$, from the OMI retrieval files with the smoothing error removed is used instead of σ_{trop} in Eqs. (4) and (6).

ACPD
14, 21749–21784, 2014

Boersma et al. (2007) suggest that the uncertainty in the tropospheric AMF is between 10–40 %. Therefore, we take the conservative estimate of $\sigma_{\mathrm{AMF_{trop}}} = 0.4 \cdot \mathrm{AMF_{trop}}$. This leads to the new retrieval error approximation of:

$$\sigma^2_{\mathrm{trop_{ak}}} = \left(\frac{\sigma_{\mathrm{total_{ran}}}}{\mathrm{AMF_{trop}}}\right)^2 + \left(\frac{0.03 X_{\mathrm{total}}}{\mathrm{AMF_{trop}}}\right)^2 + \left(\frac{0.25 \times 10^{15}}{\mathrm{AMF_{trop}}}\right)^2 + \left(0.4 N_{\mathrm{trop}}\right)^2 \quad (7)$$

All of these terms are known apart from $\sigma_{\mathrm{total_{ran}}}$. We can rearrange to calculate this based on other variables provided in the OMI product files. This leads to:

$$\left(\frac{\sigma_{\mathrm{total_{ran}}}}{\mathrm{AMF_{trop}}}\right)^2 = \sigma^2_{\mathrm{trop_{ak}}} - \left(0.4 N_{\mathrm{trop}}\right)^2 - \left(\frac{0.03 X_{\mathrm{total}}}{\mathrm{AMF_{trop}}}\right)^2 - \left(\frac{0.25 \times 10^{15}}{\mathrm{AMF_{trop}}}\right)^2 \quad (8)$$

In the rare case that the left hand side is negative, the random error component cannot be found as it would be complex, so the random error component is then set to 50 % (H. Eskes, personal communication, 2012). Now, rearranging for $\sigma_{\mathrm{total_{ran}}}$, and assuming the left hand side is positive, Eq. (8) becomes:

$$\sigma_{\mathrm{total_{ran}}} = \mathrm{AMF_{trop}} \sqrt{\left(\sigma^2_{\mathrm{trop_{ak}}}\right) - \left(0.4 N_{\mathrm{trop}}\right)^2 - \left(\frac{0.03 X_{\mathrm{total}}}{\mathrm{AMF_{trop}}}\right)^2 - \left(\frac{0.25 \times 10^{15}}{\mathrm{AMF_{trop}}}\right)^2} \quad (9)$$

This quantity was calculated for each retrieval in each grid square and then the new seasonal retrieval error was calculated taking the reduced random component into account:

$$\overline{\sigma_{\mathrm{trop_{ak}}}} = \sqrt{\left(\frac{\overline{\sigma_{\mathrm{total_{ran}}}}}{\sqrt{N}\,\overline{\mathrm{AMF_{trop}}}}\right)^2 + \left(\frac{0.03 \overline{X_{\mathrm{total}}}}{\overline{\mathrm{AMF_{trop}}}}\right)^2 + \left(\frac{0.25 \times 10^{15}}{\overline{\mathrm{AMF_{trop}}}}\right)^2 + \left(0.4 \overline{N_{\mathrm{trop}}}\right)^2} \quad (10)$$

where a bar superscript represents the seasonal time average.

ACPD
14, 21749–21784, 2014

Figure 2 shows how averaging, by decreasing the random error component, reduces the seasonal satellite tropospheric column error as calculated by our algorithm. The figure compares the simple mean of the total satellite column NO_2 error (calculated for each pixel) with our new method which reduces the estimated random error component by one over the square root of the number of observations. The reduction in the satellite column error is then presented as a percentage of the original satellite column seasonal mean error. In both summer and winter, the seasonal mean column error is reduced to 30–90 % across the domain, therefore making the OMI data much more useful for model evaluation. Only for a few retrievals over Scandinavia, does this methodology of reducing the random error component increase the overall column error (not shown here).

3 Air quality in the unified model (AQUM)

3.1 Model setup

The AQUM domain covers the UK and part of continental Europe on a rotated grid between approximately 45–60° N and 12° W–12° E. The model has a horizontal resolution of 0.11° × 0.11° with 38 vertical levels between the surface and 39 km. The model has a coupled, online tropospheric chemistry scheme using the UK Chemistry and Aerosols (UKCA) subroutines. The chemistry scheme (Regional Air Quality, RAQ) includes 40 tracers, 23 photolysis reactions and 115 gas-phase reactions (Savage et al., 2013) including the reaction of nitrate radical with formaldehyde, ethene, ethane, propane, n-butane, acetaldehyde and isoprene. The standard model setup does not include any heterogeneous chemistry. A complete chemical mechanism is included in the online supplement to Savage et al. (2013).

The model uses the Coupled Large-scale Aerosol Simulator for Studies In Climate (CLASSIC) aerosol scheme. This is a bulk aerosol scheme with the aerosols treated as an external mixture. It contains six prognostic tropospheric aerosol types: ammo-

ACPD
14, 21749–21784, 2014

nium sulphate, mineral dust, fossil fuel black carbon (FFBC), fossil fuel organic carbon (FFOC), biomass burning aerosols and ammonium nitrate. In addition, there is a diagnostic aerosol scheme for sea salt and a fixed climatology of biogenic secondary organic aerosols (BSOA). For more details of the aerosol scheme see Bellouin et al. (2011). In common with most regional AQ forecast models in Europe, AQUM shows a small negative bias for $PM_{2.5}$ and a larger negative bias for PM_{10}. For full details of the performance of the model for aerosols, NO_2 and ozone see Savage et al. (2013).

Meteorological initial conditions and lateral boundary conditions (LBCs) come from the Met Office's operational global Unified Model (25 km × 25 km) data. Initial chemical conditions come from the previous day's AQUM forecast and aerosol and chemistry LBCs come from the ECMWF GEMS (Global and regional Earth-system Monitoring using Satellite and in-situ data) reanalyses (Hollingsworth et al., 2008). The GEMS fields, available at http://www.gmes-atmosphere.eu/, provide boundary fluxes for regional air quality models such as AQUM.

This configuration of AQUM uses emission datasets from the National Atmospheric Emissions Inventory (NAEI) (1 km × 1 km) for the UK, ENTEC (5 km × 5 km) for the shipping lanes and European Monitoring and Evaluation Programme (EMEP) (50 km × 50 km) for the rest of the model domain. Over the UK the NAEI NO_x emissions datasets are made up of two source types: area and point. Area sources include traffic, light industry and urban emissions, while point sources are power stations, landfill, incinerators and refineries. Typically, the point source emissions are 100 g s^{-1} in magnitude, while the area sources tend to be 10 g s^{-1}. For most of the experiments we use 2007 instead of 2006 NO_x sources because the ENTEC shipping emissions (5 km × 5 km resolution) are available for this year, while only the coarse EMEP shipping emissions are available for the earlier years (Savage et al., 2013). The difference between 2006 and 2007 point source emissions are negligible in altering the AQUM column NO_2 (not shown). Therefore, we use the 2007 emissions datasets throughout this study. The lightning emissions are based on a parameterisation linked to the model's convection scheme. For details see O'Connor et al. (2014). We do not have a separate

ACPD
14, 21749–21784, 2014

parameterisation for soil NO_x emissions but given the large emissions from transport and industry, the soil NO_x emissions are unlikely to be important in this region.

3.2 Sensitivity experiments

We performed one control and five sensitivity experiments to investigate the AQUM's simulation of column NO_2. Two experiments used different LBCs, two experiments used modified point source emissions and two included heterogeneous chemistry. These are summarised in Table 1.

Simulation MACC investigates the sensitivity of AQUM column NO_2 to different chemical LBCs from the global Monitoring Atmospheric Composition and Climate (MACC) reanalyses, which is the follow-on project of GEMS (Inness et al., 2013). Savage et al. (2013) have undertaken a similar analysis of the MACC LBCs in AQUM. They showed that when compared with the AURN observations of O_3, AQUM-MACC performs well during the first quarter of 2006 and overestimates observations afterwards, while AQUM-GEMS has a negative bias during the first quarter of the year but compares well with observations afterwards.

We have performed additional runs to examine the impact of the point sources over the UK on NO_2 columns. The motivation behind Run E1 was to determine the impact of the NO_x point sources on the simulated column NO_2 budget, as we hypothesised that the AQUM's representation of them was the cause of the AQUM–OMI column NO_2 positive biases (see Sect. 4.1). Run E2 uses an idealised passive tracer from the point sources with a lifetime of one day to examine if the tracer columns correlated with summer AQUM-OMI positive biases (see Sect. 4.3). Runs N_2O_5High and N_2O_5Low investigate the impact of heterogeneous chemistry on NO_2 columns. Tropospheric NO_x ($NO + NO_2$) sources are dominated by anthropogenic emissions and the loss of NO_2

ACPD
14, 21749–21784, 2014

to HNO_3 is through two pathways:

$$NO_2 + OH + M \rightarrow HNO_3 + M \quad \text{(R1)}$$

$$NO_2 + O_3 \rightarrow NO_3 + O_2 \quad \text{(R2)}$$

$$NO_3 + NO_2 + M \rightleftharpoons N_2O_5 + M \quad \text{(R3)}$$

$$N_2O_5 + H_2O \xrightarrow{\text{aerosol}} 2HNO_{3(aq)} \quad \text{(R4)}$$

The standard configuration of AQUM does not include any heterogeneous reactions such as the hydrolysis of N_2O_5 on aerosol surfaces (see details of the chemistry scheme in the Supplement of Savage et al., 2013). Previous global modelling studies have shown that this process can be a significant NO_x sink at mid-latitudes in winter (e.g. Tie et al., 2003; Macintyre and Evans, 2010). Following those analyses, we have implemented this reaction, with rate k (s^{-1}) calculated as:

$$k = \frac{A\gamma\omega}{4} \quad (11)$$

where A is the aerosol surface area ($cm^2\,cm^{-3}$), γ is the uptake coefficient of N_2O_5 on aerosols (non-dimensional) and $\omega = 100\,[8RT/(\pi M)]^{\frac{1}{2}}$ ($cm\,s^{-1}$) is the root-mean-square molecular speed of N_2O_5 at temperature T (K), M is the molecular mass of N_2O_5 ($kg\,mol^{-1}$) and $R = 8.3145\,J\,mol^{-1}\,K^{-1}$.

Macintyre and Evans (2010) investigated the sensitivity of N_2O_5 loss on aerosol by using a range of uptake values (0.0, 10^{-6}, 10^{-4}, 10^{-3}, 5×10^{-3}, 10^{-2}, 2×10^{-2}, 0.1, 0.2, 0.5 and 1.0). They found that limited sensitivity occurs at low and high values of γ. At low values, the uptake pathway is an insignificant route for NO_x loss. At high values, the loss of NO_x through heterogeneous removal of N_2O_5 is limited by the rate of production of NO_3, rather than the rate of heterogeneous uptake. However, in the northern extra-tropics (including the AQUM domain), intermediate values of γ (0.001–0.02) show a significant loss of NO_x. Therefore, we experiment with $\gamma = 0.001$ and 0.02 to investigate the sensitivity of AQUM column NO_2 to heterogeneous chemistry. The

ACPD
14, 21749–21784, 2014

aerosol surface area, A, includes the contribution of seven aerosol types present in CLASSIC: sea salt aerosol, ammonium nitrate, ammonium sulphate, biomass burning aerosol, black carbon, fossil fuel organic carbon (FFOC) and biogenic secondary organic aerosol (BSOA). To account for hydroscopic growth of the aerosols, the formulation of Fitzgerald (1975) is used for growth above the deliquescence point for ammonium sulphate (RH = 81 %), sea salt (RH = 75 %) and ammonium nitrate (RH = 61 %) up to 99.5 % RH. We apply a linear fit between the efflorescence (RH = 30 % for sulphate, 42 % for sea-salt and 30 % for nitrate) and deliquescence points. There is no hydroscopic growth below the efflorescence point. Look-up tables are used for the other aerosol types. Biomass burning and FFOC aerosol growth rates are taken from Magi and Hobbs (2003), BSOA growth rates come from Varutbangkul et al. (2006) and black carbon is hydrophobic (no growth).

3.3 Statistical comparisons

For the AQUM-satellite comparisons the following model-observation statistics were used: Mean Bias (MB), Root Mean Square Error (RMSE) and the Fractional Gross Error (FGE, bounded by the values 0 to 2). These statistics are described by Han et al. (2011) and Savage et al. (2013). Further details are given in the Appendix.

4 Results

4.1 Control run

Figure 3 compares observed column NO_2 with the AQUM control Run C (with AKs applied). The AQUM and OMI averages have similar spatial patterns, with maximum and minimum column NO_2 over the urban and rural/ocean regions, respectively. In summer, AQUM and OMI background concentrations are around 0–3 $\times 10^{15}$ molecules cm^{-2}.

ACPD
14, 21749–21784, 2014

The OMI peak column NO_2 of 16–20 × 10^{15} molecules cm^{-2} is over London. AQUM simulates similar London column NO_2, but the model peak concentrations are over northern England at over 20 × 10^{15} molecules cm^{-2}. In winter, the background column NO_2 is elevated with a larger spatial extent ranging between 0–6 × 10^{15} molecules cm^{-2} in both the AQUM and OMI fields. However, the elevated AQUM background state has a larger coverage than that of OMI. Over the source regions, OMI column NO_2 peaks over London at 12–13 × 10^{15} molecules cm^{-2}, with similar concentrations seen in AQUM. However, AQUM peak column NO_2 are over northern England at 12–16 × 10^{15} molecules cm^{-2}. Therefore, independent of season, AQUM overestimates northern England column NO_2. Interestingly, the background column NO_2 is larger in winter for both AQUM and OMI, but column NO_2 is lower over the source regions in winter than summer (Pope et al., 2014).

Figure 4 shows the MB between AQUM Run C and OMI. The black polygoned regions show significant differences, i.e. where the magnitude of the MB is greater than the satellite error. In summer, there are significant positive, 5–10 × 10^{15} molecules cm^{-2}, and negative, −10 to −1 × 10^{15} molecules cm^{-2}, biases in northern England and the Benelux region, respectively. The negative biases are potentially linked to the coarser resolution EMEP NO_x emissions datasets (50 km × 50 km) which average emissions over a larger grid square causing AQUM to simulate lower column NO_2 than seen by OMI. We hypothesise that the northern England biases are linked to the point source (power station) NO_x emissions from NAEI. This is further discussed in Sect. 4.3. In winter, AQUM overestimates OMI by 1–3 × 10^{15} molecules cm^{-2} over the North Sea and Scotland, as the modelled winter background column NO_2 is larger; this is further investigated in Sect. 4.4 by including an additional NO_x sink in the chemistry scheme of the model. The northern England biases seen in summer also extend to winter, 3–5 × 10^{15} molecules cm^{-2}, suggesting the northern England biases are annual instead of seasonal. Finally, the large bias dipole in the Po Valley appears to be related to the LBCs or the winter emissions, as summer biases are small.

ACPD
14, 21749–21784, 2014

We also compared AQUM against surface observations of NO_2 from AURN, found at http://uk-air.defra.gov.uk/networks/network-info?view=aurn, and maintained by DEFRA. This was to see if there was a consistent pattern in the biases in the model column and surface NO_2. However, we find similar problems to Savage et al. (2013) where surface AQUM – observation comparisons have systematic negative biases at urban sites. The coarse model resolution, compared to the observation point measurements (even with roadside and traffic sites removed), results in significant model underestimation of NO_2 at all urban regions. Therefore, it is difficult to draw any conclusions on the AQUM skill as the model grid-point data will struggle to reproduce the point measurement observations. Also the spatial coverage of the AURN data is very sparse over the UK and AURN NO_2 measurement interferences from molybdenum converters (Steinbacher et al., 2007) overestimate surface concentrations in rural sites. Therefore, satellite (pixel area) data are the primary observations used to evaluate AQUM in this paper.

4.2 Impact of lateral boundary conditions

Figure 5a and b shows results of the sensitivity run with the MACC boundary conditions (Run MACC) and can be compared with Fig. 3a and b. The MACC LBCs have a limited impact on summer column NO_2 with peak concentrations over London and Northern England between 15–20 $\times 10^{15}$ molecules cm^{-2} for both runs MACC and C. However, in winter Run MACC increases column NO_2 from approximately 12 $\times 10^{15}$ to 16 $\times 10^{15}$ molecules cm^{-2} over the UK and Benelux region. When compared with OMI (Fig. 5a and b) the limited summer impact of the MACC LBCs results in biases which are similar to those in Fig. 4 from the control run, with biases over northern England, 5–10 $\times 10^{15}$ molecules cm^{-2}, and continental Europe, −5 to −3 $\times 10^{15}$ molecules cm^{-2}. In winter Run MACC has enhanced column NO_2 resulting in biases with OMI of between 2–5 $\times 10^{15}$ molecules cm^{-2} across the whole domain, unlike Run C with GEMS LBCs in Fig. 4. The peak positive biases are again over northern England (and the Po

ACPD
14, 21749–21784, 2014

Valley), 5×10^{15} molecules cm^{-2}, suggesting that AQUM overestimates NO_2 in the region, at the OMI overpass time, independent of season or LBCs. Therefore, the GEMs LBCs appear to give better AQUM column NO_2 forecast skill than MACC does, which is consistent with the findings of Savage et al. (2013) for the comparisons with surface ozone.

4.3 AQUM NO_x emissions sensitivity experiments

We hypothesise that significant summer Run C–OMI positive biases in northern England and Scotland (Fig. 4) are caused by the AQUM's representation of point source (mainly power station) NO_x emissions. Therefore, to better understand these biases, we investigate sensitivity experiments of NO_x emissions (Table 1) for June-July-August (JJA) 2006 (Fig. 6a shows JJA Run C–OMI positive biases). Figure 6b–d shows the JJA AQUM NO_x emissions for runs C and E1 (with point sources removed) and their difference. The peak Run C NO_x emissions are around 1.8×10^{-9} kg m^{-2} s^{-1}. However, with point sources removed, the differences are 1.8×10^{-9} kg m^{-2} s^{-1} in point source locations, showing that they make up significant part of the emissions budget.

Figure 7a and b highlights the impact of removing point sources as column NO_2 over northern England reduces from 15–25 $\times 10^{15}$ molecules cm^{-2} to 4–5 $\times 10^{15}$ molecules cm^{-2}. The Run E1–OMI MB now ranges between −10 to -6×10^{15} molecules cm^{-2}, while the Run C–OMI MB (Fig. 6a) is between 6–10 $\times 10^{15}$ molecules cm^{-2}. Therefore, the switch in sign of the biases, of similar magnitude, indicates that the point source emissions play a significant role in the AQUM column NO_2 budget.

Run E2 aimed to test whether the point sources were responsible for the positive biases in Fig. 6a by using an idealised tracer of the power station emissions. Figure 7c shows the JJA tracer column with the OMI AKs applied, where peak columns range around 16–20 $\times 10^{15}$ molecules cm^{-2} over northern England. Inspection of Figs. 6a and

ACPD
14, 21749–21784, 2014

7c suggest that the peak tracer columns overlap with the large Run C–OMI positive biases.

To test this more quantitatively, the spatial correlation between these peak concentrations from Run E2 were compared against a random tracer-MB (Run C) correlation distribution. The largest 100 tracer column pixels in Fig. 7c were compared against the MBs over the same locations in Fig. 6a, yielding a correlation of 0.45. Then, using a Monte-Carlo approach, a random 100 sample of the Fig. 6a land-based MB pixels (we use land bias pixels only as the biases in Fig. 6a are over land) were correlated against the largest 100 tracer sample. This was repeated 1000 times and then sorted from lowest to highest. The 5th and 95th percentiles were calculated at −0.162 and 0.158, respectively. Our theory is that if the point sources are responsible for the peak Run C–OMI biases, then the peak tracer concentrations, which represent the point source emissions, should be in the same location as the peak biases. By looking at the random samples correlation, we see how the tracer-MB peak value concentration compares with randomly sampled MB locations. Since 0.45 is above the 95th percentile, this shows the tracer-MB peak correlation value is significant (is actually the greatest correlation – see Fig. 7d) and that AQUM's representation of point source emissions are linked to the AQUM overestimation of column NO_2 in northern England and Scotland.

4.4 Sensitivity to heterogeneous removal of N_2O_5

Figure 8 shows the winter and summer MBs between AQUM (with LBCs from GEMS) and OMI when heterogeneous hydrolysis of N_2O_5 is implemented in the model with $\gamma = 0.001$ (Run N_2O_5Low) and $\gamma = 0.02$ (Run N_2O_5High). In the Run C summer case (see Fig. 4a) there are positive northern England and Scotland biases of around 5–10×10^{15} molecules cm^{-2}. We have shown that these positive biases are likely linked to AQUM's representation of point source emissions. However, by introducing N_2O_5 heterogeneous chemistry these positive biases are significantly reduced. In Run N_2O_5Low (Fig. 8a) there is some impact on the biases as RMSE (over UK domain 8° W–2° E

ACPD
14, 21749–21784, 2014

and 50–60° N) decreases from 3.68×10^{15} to 3.39×10^{15} molecules cm^{-2} and FGE (over UK domain 8° W–2° E and 50–60° N) also reduces slightly. In Run N_2O_5High (Fig. 8c) many of the positive biases over point sources are now insignificant and the RMSE decreases to 3.08×10^{15} molecules cm^{-2}. However, over parts of continental Europe the intensity and spread of negative biases has increased, thus suggesting that $\gamma = 0.02$ might be too strong an uptake here. The FGE does go up slightly to 0.67 and we suspect that this is due to the introduction of negative biases over relatively clean or moderately polluted areas (e.g. the Irish Sea and parts of the continent). Note that the correction of errors of large magnitude (e.g. over point sources) reduces RMSE because this metric penalises the large deviations between the model and the satellite-retrieved columns, while the introduction of errors of low magnitude over less polluted areas might increase the normalised errors given by FGE. The changes at the point source locations are most significant because of the large emissions of NO_x and aerosols suitable for this heterogeneous process to take place. Therefore, we suggest that while AQUM's representation of point sources results in the summer northern England/Scotland positive biases, including N_2O_5 heterogeneous chemistry with $\gamma = 0.02$ will partially account for this. In winter, the positive biases seen in Fig. 4b, 2–5 $\times 10^{15}$ molecules cm^{-2}, decrease as γ increases, similarly as found for summer. In Run N_2O_5Low (Fig. 8b) the spatial spread of significantly positive biases is only partially reduced, resulting in small decreases of RMSE (from 5.12×10^{15} to 5.05×10^{15} molecules cm^{-2}) and FGE (from 0.63 to 0.62). For Run N_2O_5High (Fig. 8d) the cluster of significantly positive biases has decreased spatially yielding the best comparisons, with RMSE and FGE values of 4.48×10^{15} molecules cm^{-2} and 0.60, respectively.

5 Conclusions

We have successfully used OMI satellite observations of column NO_2 over the UK to further explore the AQUM performance, extending on previous validation of the model

ACPD
14, 21749–21784, 2014

which had only used surface data. In order to do this we have looked in detail at the satellite errors (random, systematic and smoothing) and derived an algorithm which reduces the retrieval random error component when averaging retrievals. This allows more critical AQUM-satellite comparisons as the time average random error component can be reduced by 30–90 % in all seasons.

Based on the summer and winter comparisons, the standard (operational) AQUM overestimates column NO_2 over northern England/Scotland by 5–10×10^{15} molecules cm^{-2} and over the northern domain by 2–5×10^{15} molecules cm^{-2}. The use of a different set of lateral boundary conditions (from the MACC reanalysis), which are known to increase AQUM's surface ozone positive bias (Savage et al., 2013), also increases the error in the NO_2 columns. The AQUM column NO_2 is increased, especially in winter, by 2–5×10^{15} molecules cm^{-2}, resulting in poorer comparisons with OMI.

From multiple sensitivity experiments on the UK NO_x point source emissions we conclude that it was AQUM's representation of these emissions which caused the northern England/Scotland summer biases. By emitting an idealised tracer in the NO_x points sources we found a significant correlation of the peak tracer columns to the AQUM – OMI MBs. Finally, introducing N_2O_5 heterogeneous chemistry in AQUM improves the AQUM–OMI comparisons in both seasons. In winter, the spatial extent of positive biases, 2–5×10^{15} molecules cm^{-2}, decreases. In summer, the northern England biases decrease both spatially and in magnitude from 5–10 to 0–5×10^{15} molecules cm^{-2}. Therefore, this suggests that in summer the AQUM's representation of NO_x point sources is inaccurate but can be partially masked by the introduction of N_2O_5 heterogeneous chemistry.

As this study has shown the potential use of satellite observations, along with the time-averaged random error algorithm, to evaluate AQUM, the data could be used in future to evaluate operation air quality forecasts. We also show that the heterogeneous loss of N_2O_5 on aerosol is an important sink of NO_2 and should be included in the operational AQUM.

ACPD
14, 21749–21784, 2014

Appendix A

The equations for mean bias (MB), root mean square error (RMSE), modified normalised mean bias (MNMB) and the fractional gross error (FGE) are given here, where f is the model output, o is the satellite measurements, N is the total number of elements and i is the index. Mean Bias (MB):

$$\mathrm{MB} = \frac{1}{N}\sum_{i}(f_i - o_i) \tag{A1}$$

Modified Normalised Mean Bias (MNMB):

$$\mathrm{MNMB} = \frac{2}{N}\sum\frac{(f_i - o_i)}{f_i + o_i} \tag{A2}$$

Root Mean Square Error (RMSE):

$$\mathrm{RMSE} = \sqrt{\frac{1}{N}\sum_{i}(f_i - o_i)^2} \tag{A3}$$

Fractional Gross Error (FGE):

$$\mathrm{FGE} = \frac{2}{N}\sum_{i}\left|\frac{f_i - o_i}{f_i + o_i}\right| \tag{A4}$$

Acknowledgements. We acknowledge the use of the Tropospheric Emissions Monitoring Internet Service (TEMIS) OMI dataset used in this study. This work was supported by the UK Natural Environment Research Council (NERC) and National Centre for Earth Observation (NCEO). Richard Pope thanks the NCEO for a Ph.D. studentship to undertake this work. We are grateful to Ben Johnson of the Met Office who provided advice for the implementation of aerosol growth and surface area diagnostics in CLASSIC.

ACPD
14, 21749–21784, 2014

References

Bellouin, N., Rae, J., Jones, A., Johnson, C., Haywood, J., and Boucher, O.: Aerosol forcing in the Climate Model Intercomparison Project (CMIP5) simulations by HadGEM2-ES and the role of ammonium nitrate, J. Geophys. Res.-Atmos., 116, D20206, doi:10.1029/2011JD016074, 2011. 21760

Blond, N., Boersma, K. F., Eskes, H. J., van der A, R. J., Van Roozendael, M., De Smedt, I., Bergametti, G., and Vautard, R.: Intercomparison of SCIAMACHY nitrogen dioxide observations, in situ measurements and air quality modeling results over Western Europe, J. Geophys. Res.-Atmos., 112, D10311, doi:10.1029/2006JD007277, 2007. 21752

Boersma, K., Eskes, H., and Brinksma, E.: Error analysis for tropospheric NO_2 retrieval from space, J. Geophys. Res.-Atmos., 109, D04311, doi:10.1029/2003JD003962, 2004. 21756, 21757

Boersma, K. F., Eskes, H. J., Veefkind, J. P., Brinksma, E. J., van der A, R. J., Sneep, M., van den Oord, G. H. J., Levelt, P. F., Stammes, P., Gleason, J. F., and Bucsela, E. J.: Near-real time retrieval of tropospheric NO_2 from OMI, Atmos. Chem. Phys., 7, 2103–2118, doi:10.5194/acp-7-2103-2007, 2007. 21758

Boersma, K., Jacob, D., Bucsela, E., Perring, A., Dirksen, R., van der A, R., Yantosca, R., Park, R., Wenig, M., Bertram, T., and Cohen, R.: Validation of {OMI} tropospheric {NO2} observations during INTEX-B and application to constrain emissions over the eastern United States and Mexico, Atmos. Environ., 42, 4480–4497, doi:10.1016/j.atmosenv.2008.02.004, 2008. 21753, 21754

Boersma, K. F., Jacob, D. J., Trainic, M., Rudich, Y., DeSmedt, I., Dirksen, R., and Eskes, H. J.: Validation of urban NO_2 concentrations and their diurnal and seasonal variations observed from the SCIAMACHY and OMI sensors using in situ surface measurements in Israeli cities, Atmos. Chem. Phys., 9, 3867–3879, doi:10.5194/acp-9-3867-2009, 2009. 21752

Boersma, K., Braak, R., and van der A, R.: Dutch OMI NO_2 (DOMINO) data product v2.0, Tropospheric Emissions Monitoring Internet Service on-line Documentation, available at: http://www.temis.nl/docs/OMI_NO2_HE5_2.0_2011.pdf (last access: June 2014), KNMI, the Netherlands, 2011a. 21753, 21755

Boersma, K. F., Eskes, H. J., Dirksen, R. J., van der A, R. J., Veefkind, J. P., Stammes, P., Huijnen, V., Kleipool, Q. L., Sneep, M., Claas, J., Leitão, J., Richter, A., Zhou, Y., and Brunner, D.:

ACPD
14, 21749–21784, 2014

An improved tropospheric NO_2 column retrieval algorithm for the Ozone Monitoring Instrument, Atmos. Meas. Tech., 4, 1905–1928, doi:10.5194/amt-4-1905-2011, 2011b. 21753
Braak, R.: Row Anomaly Flagging Rules Lookup Table, KNMI Technical Document TN-OMIE-KNMI-950, KNMI, the Netherlands, 2010. 21754
Curier, R., Kranenburg, R., Segers, A., Timmermans, R., and Schaap, M.: Synergistic use of {OMI} {NO_2} tropospheric columns and LOTOS?EUROS to evaluate the {NO_x} emission trends across Europe, Remote Sens. Environ., 149, 58–69, doi:10.1016/j.rse.2014.03.032, 2014. 21752
DEFRA: Automatic Urban and Rural Network (AURN), available at: http://uk-air.defra.gov.uk/networks/network-info?view=aurn (last access: 2014), DEFRA, UK, 2012.
Eskes, H. J. and Boersma, K. F.: Averaging kernels for DOAS total-column satellite retrievals, Atmos. Chem. Phys., 3, 1285–1291, doi:10.5194/acp-3-1285-2003, 2003. 21754
Fitzgerald, J. W.: Approximation formulas for the equilibrium size of an aerosol particle as a function of its dry size and composition and the ambient relative humidity, J. Appl. Meteorol., 14, 1044–1049, 1975. 21763
Foley, K. M., Roselle, S. J., Appel, K. W., Bhave, P. V., Pleim, J. E., Otte, T. L., Mathur, R., Sarwar, G., Young, J. O., Gilliam, R. C., Nolte, C. G., Kelly, J. T., Gilliland, A. B., and Bash, J. O.: Incremental testing of the Community Multiscale Air Quality (CMAQ) modeling system version 4.7, Geosci. Model Dev., 3, 205–226, doi:10.5194/gmd-3-205-2010, 2010. 21752
Han, K., Lee, C., Lee, J., Kim, J., and Song, C.: A comparison study between model-predicted and OMI-retrieved tropospheric NO_2 columns over the Korean peninsula, Atmos. Environ., 45, 2962–2971, 2011. 21752, 21763
HoC: House of Commons Environmental Audit Report (HCEA): Air Quality: Vol 1 (2009–2010), availabale at: http://www.publications.parliament.uk/pa/cm200910/cmselect/cmenvaud/229/229i.pdf (last access: February 2014), House of Commons, London, UK, 2010. 21751
Hollaway, M. J., Arnold, S. R., Challinor, A. J., and Emberson, L. D.: Intercontinental transboundary contributions to ozone-induced crop yield losses in the Northern Hemisphere, Biogeosciences, 9, 271–292, doi:10.5194/bg-9-271-2012, 2012. 21751
Hollingsworth, A., Engelen, R., Benedetti, A., Dethof, A., Flemming, J., Kaiser, J., Morcrette, J., Simmons, A., Textor, C., Boucher, O., Chevallier, F., Rayner, P., Elbern, H., Eskes, H., Granier, C., Peuch, V.-H., Rouil, L., and Schultz, M. G.: Toward a monitoring and forecasting system for atmospheric composition: the GEMS project, B. Am. Meteorol. Soc., 89, 1147–1164, 2008. 21760

ACPD
14, 21749–21784, 2014

Huijnen, V., Eskes, H. J., Poupkou, A., Elbern, H., Boersma, K. F., Foret, G., Sofiev, M., Valdebenito, A., Flemming, J., Stein, O., Gross, A., Robertson, L., D'Isidoro, M., Kioutsioukis, I., Friese, E., Amstrup, B., Bergstrom, R., Strunk, A., Vira, J., Zyryanov, D., Maurizi, A., Melas, D., Peuch, V.-H., and Zerefos, C.: Comparison of OMI NO_2 tropospheric columns with an ensemble of global and European regional air quality models, Atmos. Chem. Phys., 10, 3273–3296, doi:10.5194/acp-10-3273-2010, 2010. 21751, 21755

Inness, A., Baier, F., Benedetti, A., Bouarar, I., Chabrillat, S., Clark, H., Clerbaux, C., Coheur, P., Engelen, R. J., Errera, Q., Flemming, J., George, M., Granier, C., Hadji-Lazaro, J., Huijnen, V., Hurtmans, D., Jones, L., Kaiser, J. W., Kapsomenakis, J., Lefever, K., Leitão, J., Razinger, M., Richter, A., Schultz, M. G., Simmons, A. J., Suttie, M., Stein, O., Thépaut, J.-N., Thouret, V., Vrekoussis, M., Zerefos, C., and the MACC team: The MACC reanalysis: an 8 yr data set of atmospheric composition, Atmos. Chem. Phys., 13, 4073–4109, doi:10.5194/acp-13-4073-2013, 2013. 21761

Irie, H., Kanaya, Y., Akimoto, H., Tanimoto, H., Wang, Z., Gleason, J. F., and Bucsela, E. J.: Validation of OMI tropospheric NO_2 column data using MAX-DOAS measurements deep inside the North China Plain in June 2006: Mount Tai Experiment 2006, Atmos. Chem. Phys., 8, 6577–6586, doi:10.5194/acp-8-6577-2008, 2008. 21754

Lauer, A., Dameris, M., Richter, A., and Burrows, J. P.: Tropospheric NO_2 columns: a comparison between model and retrieved data from GOME measurements, Atmos. Chem. Phys., 2, 67–78, doi:10.5194/acp-2-67-2002, 2002. 21751

Macintyre, H. L. and Evans, M. J.: Sensitivity of a global model to the uptake of N_2O_5 by tropospheric aerosol, Atmos. Chem. Phys., 10, 7409–7414, doi:10.5194/acp-10-7409-2010, 2010. 21762

Magi, B. I. and Hobbs, P. V.: Effects of humidity on aerosols in southern Africa during the biomass burning season, J. Geophys. Res.-Atmos., 108, 8495, doi:10.1029/2002JD002144, 2003. 21763

Monks, S., Arnold, S., and Chipperfield, M.: Evidence for El Niño–Southern Oscillation (ENSO) influence on Arctic CO interannual variability through biomass burning emissions, Geophys. Res. Lett., 39, L14804, doi:10.1029/2012GL052512, 2012. 21751

O'Connor, F. M., Johnson, C. E., Morgenstern, O., Abraham, N. L., Braesicke, P., Dalvi, M., Folberth, G. A., Sanderson, M. G., Telford, P. J., Voulgarakis, A., Young, P. J., Zeng, G., Collins, W. J., and Pyle, J. A.: Evaluation of the new UKCA climate-composition model –

ACPD
14, 21749–21784, 2014

Part 2: The Troposphere, Geosci. Model Dev., 7, 41–91, doi:10.5194/gmd-7-41-2014, 2014. 21760

Pope, R., Savage, N., Chipperfield, M., Arnold, S., and Osborn, T.: The influence of synoptic weather regimes on UK air quality: analysis of satellite column NO_2, Atmos. Sci. Lett., 15, 211–217, doi:10.1002/asl2.492, 2014. 21764

Savage, N. H., Pyle, J. A., Braesicke, P., Wittrock, F., Richter, A., Nüß, H., Burrows, J. P., Schultz, M. G., Pulles, T., and van Het Bolscher, M.: The sensitivity of Western European NO_2 columns to interannual variability of meteorology and emissions: a model – GOME study, Atmos. Sci. Lett., 9, 182–188, 2008. 21751

Savage, N. H., Agnew, P., Davis, L. S., Ordóñez, C., Thorpe, R., Johnson, C. E., O'Connor, F. M., and Dalvi, M.: Air quality modelling using the Met Office Unified Model (AQUM OS24-26): model description and initial evaluation, Geosci. Model Dev., 6, 353–372, doi:10.5194/gmd-6-353-2013, 2013. 21751, 21752, 21753, 21759, 21760, 21761, 21762, 21763, 21765, 21766, 21769

Seigneur, C., Pun, B., Pai, P., Louis, J.-F., Solomon, P., Emery, C., Morris, R., Zahniser, M., Worsnop, D., Koutrakis, P., White, W., and Tombach, I.: Guidance for the performance evaluation of three-dimensional air quality modeling systems for particulate matter and visibility, J. Air Waste Manage., 50, 588–599, 2000. 21752

Steinbacher, M., Zellweger, C., Schwarzenbach, B., Bugmann, S., Buchmann, B., Ordonez, C., Prevot, A., and Hueglin, C.: Nitrogen oxide measurements at rural sites in Switzerland: bias of conventional measurement techniques, J. Geophys. Res.-Atmos., 112, D11307, doi:10.1029/2006JD007971, 2007. 21765

Tie, X., Emmons, L., Horowitz, L., Brasseur, G., Ridley, B., Atlas, E., Stround, C., Hess, P., Klonecki, A., Madronich, S., Talbot, R., and Dibb, J.: Effect of sulfate aerosol on tropospheric NO_x and ozone budgets: model simulations and TOPSE evidence, J. Geophys. Res.-Atmos., 108, 2156–2202, doi:10.1029/2001JD0015082003. 21762

van Noije, T. P. C., Eskes, H. J., Dentener, F. J., Stevenson, D. S., Ellingsen, K., Schultz, M. G., Wild, O., Amann, M., Atherton, C. S., Bergmann, D. J., Bey, I., Boersma, K. F., Butler, T., Cofala, J., Drevet, J., Fiore, A. M., Gauss, M., Hauglustaine, D. A., Horowitz, L. W., Isaksen, I. S. A., Krol, M. C., Lamarque, J.-F., Lawrence, M. G., Martin, R. V., Montanaro, V., Müller, J.-F., Pitari, G., Prather, M. J., Pyle, J. A., Richter, A., Rodriguez, J. M., Savage, N. H., Strahan, S. E., Sudo, K., Szopa, S., and van Roozendael, M.: Multi-model ensemble simula-

ACPD
14, 21749–21784, 2014

tions of tropospheric NO_2 compared with GOME retrievals for the year 2000, Atmos. Chem. Phys., 6, 2943–2979, doi:10.5194/acp-6-2943-2006, 2006. 21751

Varutbangkul, V., Brechtel, F. J., Bahreini, R., Ng, N. L., Keywood, M. D., Kroll, J. H., Flagan, R. C., Seinfeld, J. H., Lee, A., and Goldstein, A. H.: Hygroscopicity of secondary organic aerosols formed by oxidation of cycloalkenes, monoterpenes, sesquiterpenes, and related compounds, Atmos. Chem. Phys., 6, 2367–2388, doi:10.5194/acp-6-2367-2006, 2006. 21763

Velders, G. J., Granier, C., Portmann, R. W., Pfeilsticker, K., Wenig, M., Wagner, T., Platt, U., Richter, A., and Burrows, J. P.: Global tropospheric NO_2 column distributions: comparing three-dimensional model calculations with GOME measurements, J. Geophys. Res.-Atmos., 106, 12643–12660, 2001. 21751

WHO: Air Quality and Health, available at: http://www.who.int/mediacentre/factsheets/fs313/en/ (last access: February 2014), World Health Organisation, Geneva, Switzerland, 2011. 21751

ACPD
14, 21749–21784, 2014

Table 1. List of AQUM runs and experiments.

Run ID	Run Description
C	Control run (GEMS LBCs)
MACC	MACC LBCs
E1	No point sources emissions
E2	Idealised point source tracer
N_2O_5Low	With N_2O_5 heterogeneous chemistry with $\gamma = 0.001$
N_2O_5High	As run N_2O_5Low but with $\gamma = 0.02$

ACPD
14, 21749–21784, 2014

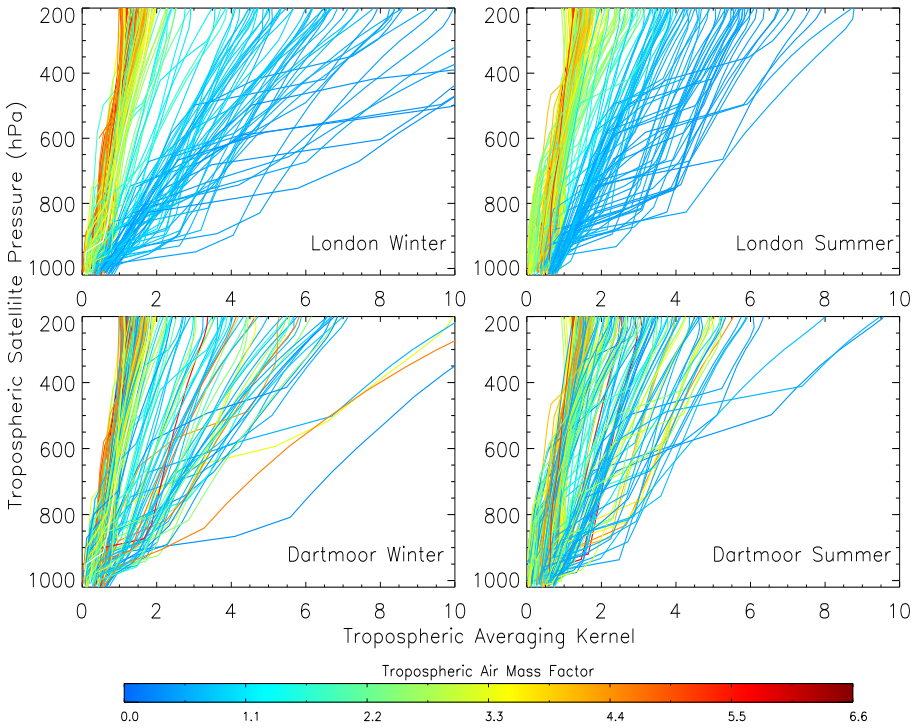

Figure 1. Example OMI averaging kernels for London (top) and Dartmoor (bottom) for summer (right) and winter (left) 2006. Averaging kernels have been coloured to their respective tropospheric air mass factor values.

ACPD
14, 21749–21784, 2014

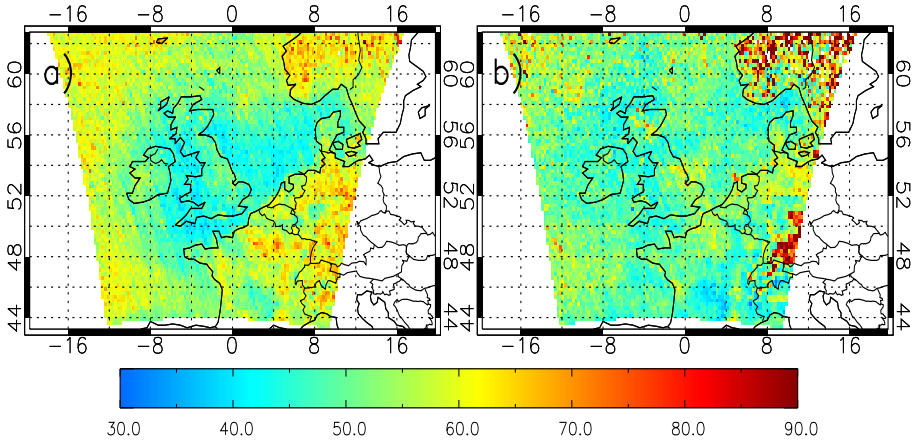

Figure 2. New seasonal satellite mean error, obtained by reduction of random error using the methodology described in Sect. 2, as a percentage of simple seasonal mean of satellite total error for 2006. Smoothing errors have been removed. **(a)** Summer and **(b)** winter.

ACPD
14, 21749–21784, 2014

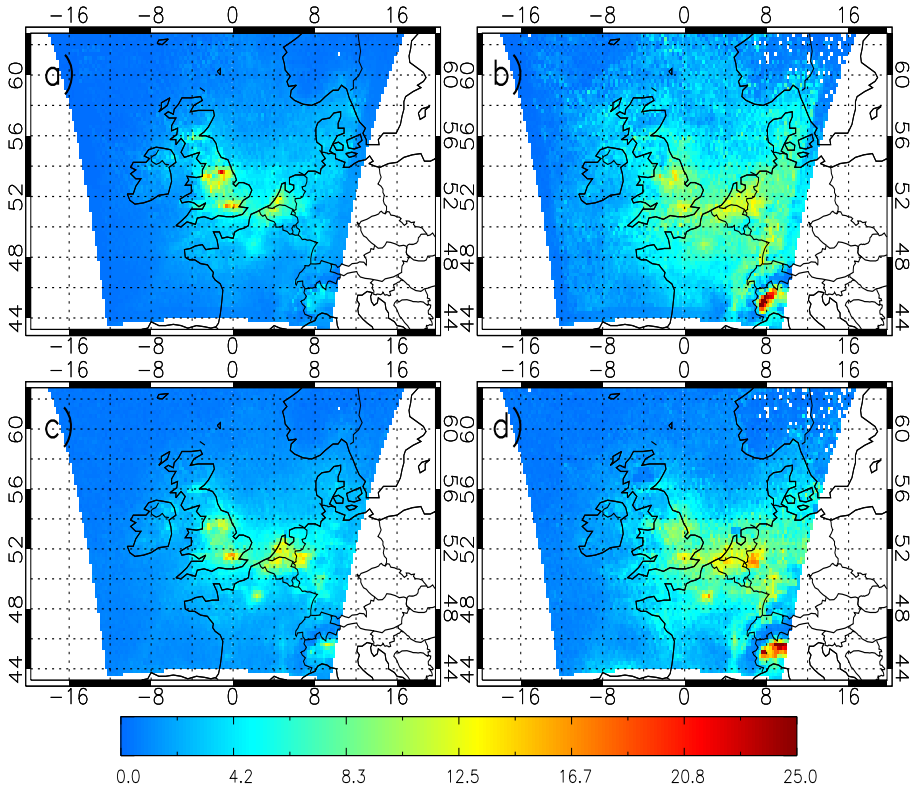

Figure 3. Tropospheric NO_2 column ($\times 10^{15}$ molecules cm^{-2}), 2006, for **(a)** AQUM Run C (with averaging kernels (AK) applied) summer, **(b)** AQUM Run C (AKs applied) winter, **(c)** OMI summer and **(d)** OMI winter.

ACPD
14, 21749–21784, 2014

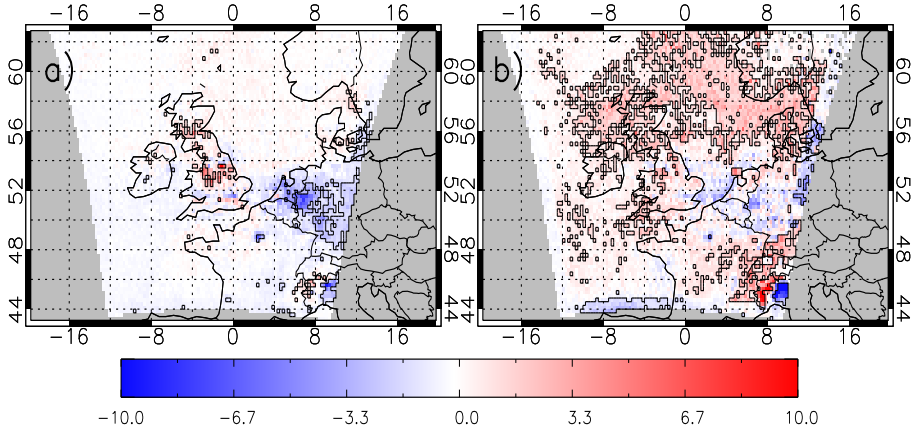

Figure 4. Mean bias in tropospheric NO_2 column ($\times 10^{15}$ molecules cm^{-2}), 2006, between AQUM Run C (AKs applied) and OMI for **(a)** summer (RMSE = 3.68 $\times 10^{15}$ molecules cm^{-2} and FGE = 0.65) and **(b)** winter (RMSE = 5.12 $\times 10^{15}$ molecules cm^{-2} and FGE = 0.63). The RMSE and FGE are over the UK between 8° W–2° E and 50–60° N and black polygoned regions show significant differences. Also the same for mean bias plots in Figs. 5–8.

ACPD
14, 21749–21784, 2014

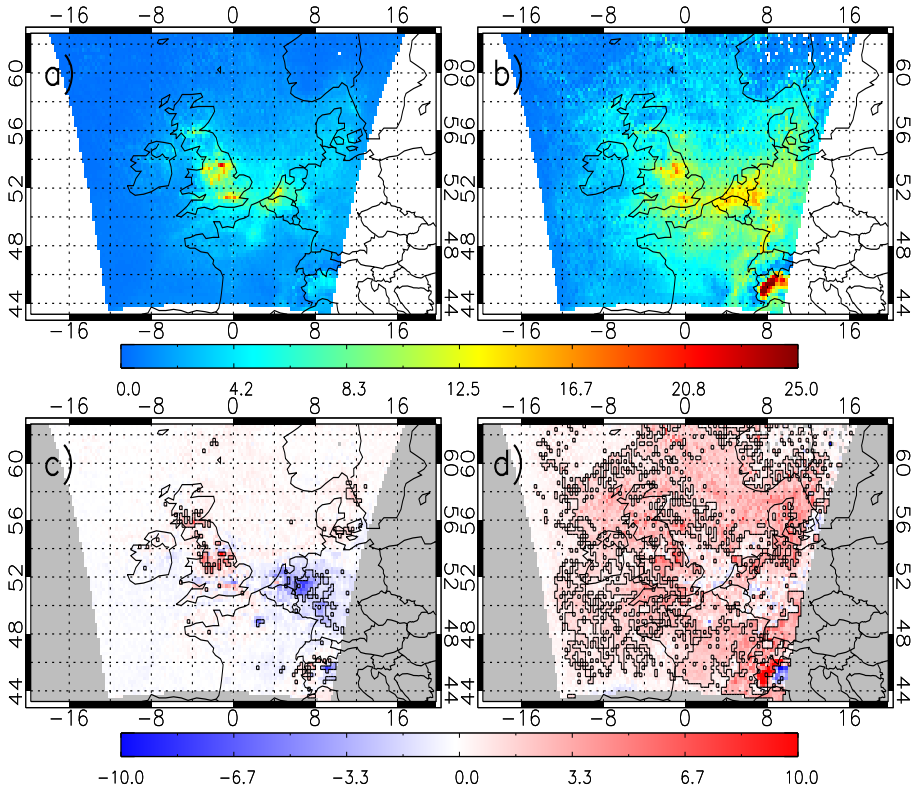

Figure 5. Tropospheric NO_2 column ($\times 10^{15}$ molecules cm^{-2}), 2006, from AQUM Run MACC (AKs applied) for **(a)** summer and **(b)** winter. AQUM Run MACC (AKs applied) and OMI mean bias for **(c)** summer (RMSE = 3.74 $\times 10^{15}$ molecules cm^{-2} and FGE = 0.63) and **(d)** winter (RMSE = 6.00 $\times 10^{15}$ molecules cm^{-2} and FGE = 0.65).

ACPD
14, 21749–21784, 2014

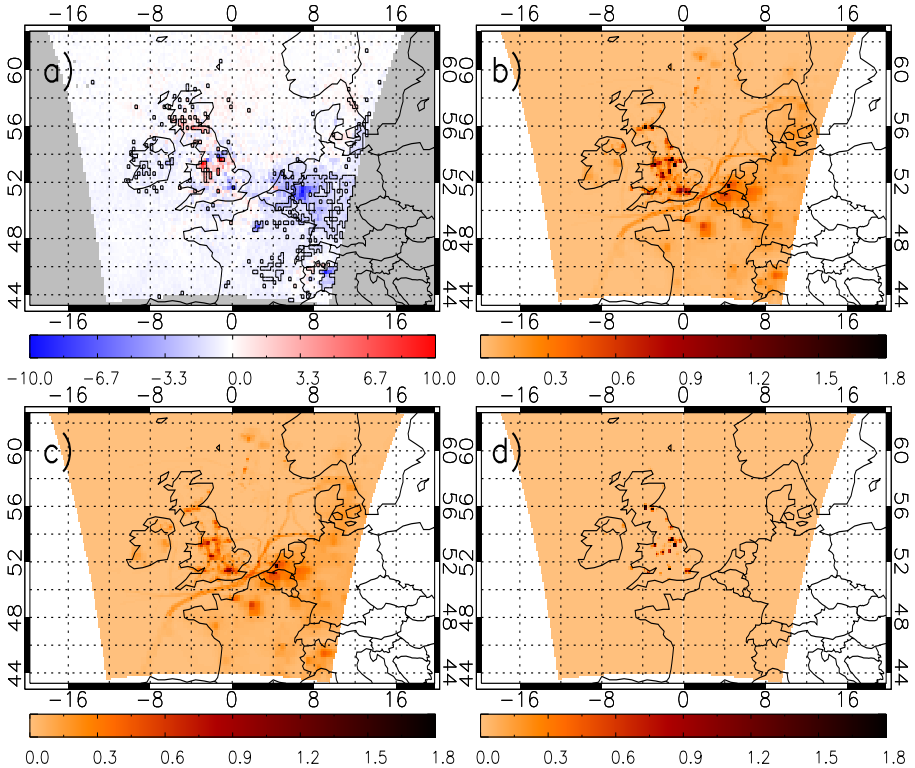

Figure 6. AQUM Run C (AKs applied)–OMI tropospheric NO_2 column ($\times 10^{15}$ molecules cm^{-2}) JJA 2006 mean bias. These are the control MBs to compare to the point source sensitivity experiments (RMSE = 3.64 $\times 10^{15}$ molecules cm^{-2} and FGE = 0.66). NO_x emissions ($\times 10^{-9}$ kg m^{-2} s^{-1}), JJA 2006, used in AQUM for **(b)** Run C and **(c)** Run E1. **(d)** shows the difference between **(b)** and **(c)**.

ACPD
14, 21749–21784, 2014

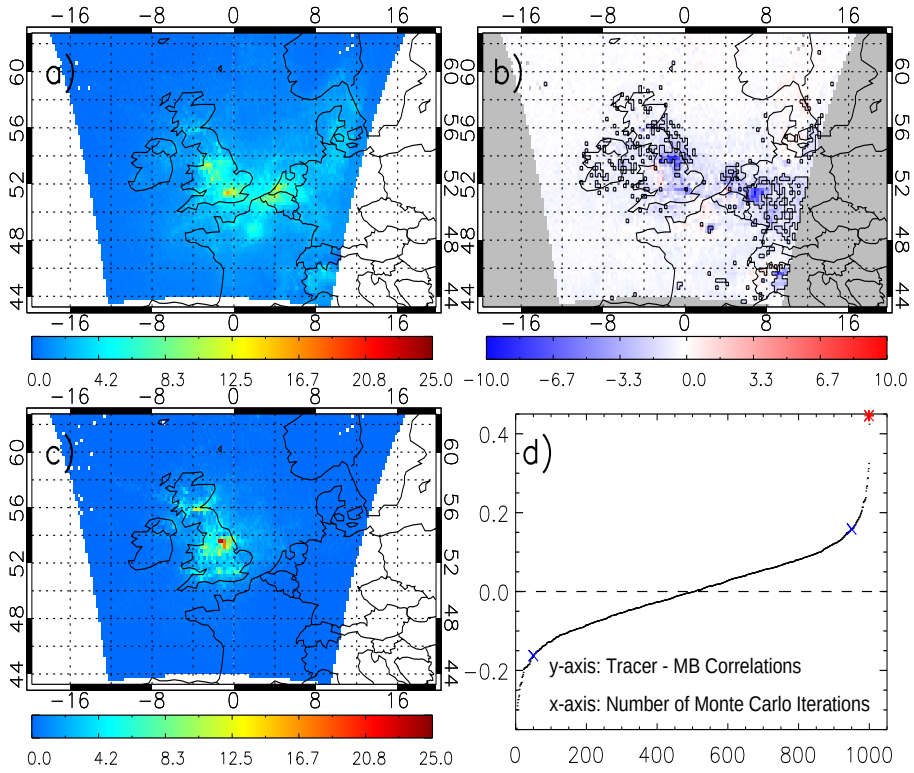

Figure 7. Tropospheric column ($\times 10^{15}$ molecules cm^{-2}), JJA 2006, for **(a)** AQUM Run E1 NO_2 (AKs applied), **(b)** AQUM Run E1 NO_2 (AKs applied)–OMI (RMSE = 3.02 $\times 10^{15}$ molecules cm^{-2} and FGE = 0.68) and **(c)** AQUM Run E2 Tracer (AKs applied). **(d)** Peak Run E2 and co-located Run C–OMI MB correlation (red star) significance distribution. Black dots are Run E2 and random Run C–OMI MB correlations. Blue X = 5th and 95th percentiles of the 1000 size sample.

ACPD
14, 21749–21784, 2014

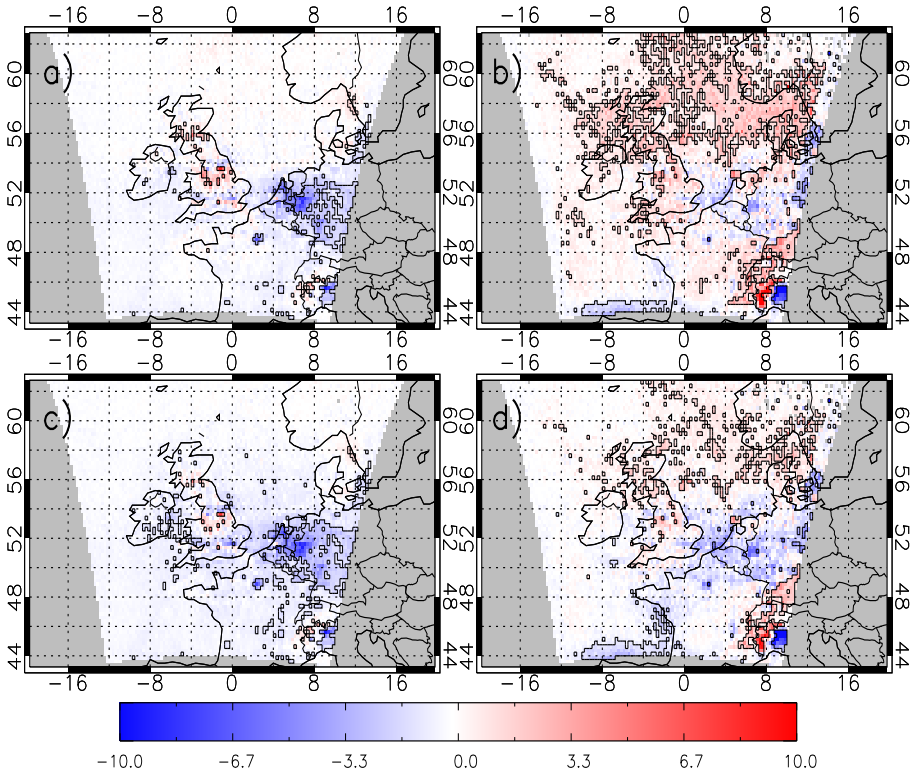

Figure 8. MB in tropospheric NO_2 column ($\times 10^{15}$ molecules cm^{-2}), 2006, between AQUM (AKs applied)–OMI for **(a)** summer $\gamma = 0.001$ (RMSE = 3.39×10^{15} molecules cm^{-2} and FGE = 0.65), **(b)** winter $\gamma = 0.001$ (RMSE = 5.05×10^{15} molecules cm^{-2} and FGE = 0.62), **(c)** summer $\gamma = 0.02$ (RMSE = 3.08×10^{15} molecules cm^{-2} and FGE = 0.67) and **(d)** winter $\gamma = 0.02$ (RMSE = 4.48×10^{15} molecules cm^{-2} and FGE = 0.60).

ACPD
14, 21749–21784, 2014